

Emergence of large quantum oscillation frequencies in thin flakes of the kagome superconductor CsV₃Sb₅

W. Zhang^{§,1}, Lingfei Wang^{§,1}, Chun Wai Tsang,¹ Xinyou Liu,¹
Jiayu Xie,¹ Wing Chi Yu,^{2,*} Kwing To Lai,^{1,3,†} and Swee K. Goh^{1,‡}

¹*Department of Physics, The Chinese University of Hong Kong, Shatin, Hong Kong, China*

²*Department of Physics, City University of Hong Kong, Kowloon, Hong Kong, China*

³*Shenzhen Research Institute, The Chinese University of Hong Kong, Shatin, Hong Kong, China*

(Dated: November 1, 2022)

Kagome metals AV₃Sb₅ (A = K, Rb, Cs) are recently discovered platforms featuring an unusual charge-density-wave (CDW) order and superconductivity. The electronic band structure of a kagome lattice can host both flat bands as well as Dirac-like bands, offering the possibility to stabilize various quantum states. Here, we probe the band structure of CsV₃Sb₅ via Shubnikov-de Haas quantum oscillations on both bulk single crystals and thin flakes. Although our frequency spectra are broadly consistent with the published data, we unambiguously reveal the existence of new frequencies with large frequencies ranging from ~ 2085 T to ~ 2717 T in thin flakes when the magnetic field is along the *c*-axis. These quasi-two-dimensional frequencies correspond to $\sim 52\%$ to 67% of the CDW-distorted Brillouin zone volume. The Lifshitz-Kosevich analysis further uncovers surprisingly small cyclotron effective masses, of the order of $\sim 0.1 m_e$, for these frequencies. Consequently, a large number of high-velocity carriers exists in the thin flake of CsV₃Sb₅. Comparing with our band structure calculations, we argue that an orbital-selective modification of the band structure is active. Our results provide indispensable information for understanding the fermiology of CsV₃Sb₅, paving a way for understanding how an orbital-selective mechanism can become an effective means to tune its electronic properties.

I. INTRODUCTION

In a kagome lattice, the geometric frustration of the local moments provide a unique platform for the search of quantum spin liquid state¹. Besides magnetism, the band structure of the kagome lattice naturally contains linearly dispersive Dirac cones, flat bands and van Hove singularities^{2–4}. While the Dirac cones feature non-trivial topological properties, the flat bands and the van Hove singularities promote the strong electronic correlation. The combination of geometric frustration, non-trivial topology and strong correlation in the kagome lattice provides an ideal platform to study exotic quantum phenomena, such as giant anomalous Hall effect in a ferromagnetic kagome metal Co₃Sn₂S₂⁵.

Recently, the discovery of kagome metals AV₃Sb₅ (A=K, Rb, Cs) has attracted a great deal of interest owing to the interplay among charge order, superconductivity and non-trivial topology^{6,7}. They all show a second-order transition at $T_{\text{CDW}} \sim 80\text{--}100$ K, which is attributed to the appearance of a charge-density-wave (CDW) phase^{8–21}. Growing evidence was found to support the idea that the CDW phase could have an unconventional origin, including the observation of the chiral charge order^{17,22,23} and the possible time-reversal symmetry breaking without local moments^{24–26}. In addition, the appearance of an anomalous Hall effect, which is associated with the CDW transition, is also believed to support the scenario of an unconventional CDW state^{27–29}. At lower temperatures, a superconducting transition has been found in all members of AV₃Sb₅ at $T_c \sim 0.9\text{--}2.5$ K^{30–32}. Upon the application of pressure, a double-peak superconducting dome is observed in the phase dia-

grams of CsV₃Sb₅^{9,33–35} and RbV₃Sb₅³⁶, despite the fact that T_{CDW} is monotonically decreasing with pressure. This suggests an unusual competition between CDW and superconductivity.

To gain a deeper understanding of the CDW and superconductivity in AV₃Sb₅, a thorough knowledge of the Fermi surface is indispensable. Quantum oscillation (QO) investigations are one of the powerful tools to probe the Fermi surface and extract the quasiparticle effective mass, which have successfully revealed the Fermi surface topology of some candidates of topological semimetals^{37–40}. To date, several QO reports already emerged in bulk single crystals of CsV₃Sb₅^{28,33,41–46}. In all these reports, several low-frequency oscillations below ~ 100 T, which correspond to small Fermi surface areas, have been consistently observed when the magnetic field (*B*) is along the crystalline *c*-axis. Furthermore, these frequencies are also found to have a low effective mass, and consequently they have been associated with Fermi surfaces originated from the Dirac cones. The non-trivial topological nature of some of these small frequencies were further confirmed via analyzing the phase of quantum oscillations⁴¹. Ortiz *et al.*⁴² and Shrestha *et al.*⁴⁶ further reported a rich spectrum featuring several peaks ranging from 500 T to 2000 T when $B \parallel c$ (hereafter termed the “mid-frequency spectrum” for the ease of discussion), allowing the authors to discuss the impact of the CDW order on the Fermi surface topography, and to confirm the topologically nontrivial and quasi-2D nature of Fermi surfaces.

The fact that the mid-frequency spectrum has not been detected consistently across the existing reports, despite a rather satisfactory agreement on the low-frequency

spectrum, is most likely due to exceedingly weak signals from the mid-frequency oscillations. Thus, the QO endeavour of CsV_3Sb_5 is far from completed, and boosting the QO signal strength is a route for further discovery. Arming with this central guiding principle, we study single crystals of CsV_3Sb_5 with a large residual resistance ratio (RRR, defined as $R(300\text{ K})/R(5\text{ K})$). We further isolate thin flakes from these single crystals for detailed investigations. In this manuscript, we report the discovery of clear Shubnikov-de Haas (SdH) QO frequencies far beyond 2000 T (naturally termed “high-frequency spectrum”) in our thin flakes. The magnetic field angle dependence of these frequencies shows that they come from quasi-two dimensional (2D) Fermi surface sheets. Interestingly, these high-frequency peaks are found to host very small effective masses on the order of $0.1 m_e$, where m_e is the free-electron mass. Thus, our results provide new fermiology insights for CsV_3Sb_5 in a carefully designed QO experiment, and unravel the existence of a large number of high-mobility carriers that are pivotal for exotic quantum transport phenomena in CsV_3Sb_5 .

II. METHODS

High-quality single crystals of CsV_3Sb_5 were synthesized from Cs (ingot, 99.95 %), V (powder, 99.9 %) and Sb (shot, 99.9999 %) using self-flux method similar to Refs. 6 and 30. In this study, we sealed the raw materials inside a pure-Ar-filled stainless steel jacket with the molar ratio of Cs:V:Sb = 7:3:14. The as-grown single crystals were millimeter-sized shiny plates, as shown in the inset of Fig. 1. Magnetotransport properties were measured by a standard four-terminal configuration in a Physical Property Measurement System by Quantum Design. Dupont 6838 silver paste was used for making the electrical contacts on bulk crystals, while a set of patterned electrodes was used to form a tight contact with thin flakes exfoliated from the bulk crystals⁴⁷. The thickness of the thin flakes was determined by a dual-beam focused ion beam system (Scios 2 DualBeam by Thermo Scientific). A Stanford Research 830 lock-in amplifier was used for QO measurements. Density functional theory (DFT) calculations were performed, with details provided in Supplemental Material⁴⁸.

III. RESULTS

A. Shubnikov-de Haas quantum oscillations in bulk samples

Figure 1(a) shows the temperature dependence of the electrical resistivity ($\rho(T)$) for our high-quality single-crystalline CsV_3Sb_5 in the bulk form. On cooling, $\rho(T)$ decreases and an anomaly appears at around 95 K. Correspondingly, a peak appears in $d\rho/dT$, as displayed in Fig. 1(b), which is consistent with the reported CDW

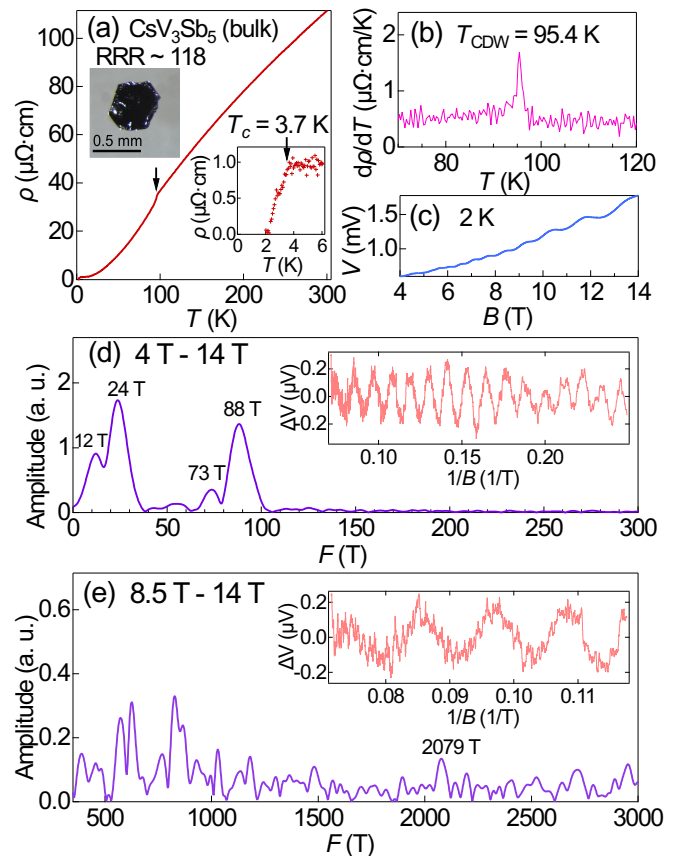


FIG. 1. (a) Temperature dependence of electrical resistivity for the bulk CsV_3Sb_5 with a RRR of 118. The upper inset is the photograph of a typical CsV_3Sb_5 single crystal and the lower inset shows the superconducting transition. (b) Temperature dependence of $d\rho/dT$, displaying a sharp peak at T_{CDW} . (c) Raw data of the lock-in voltage versus magnetic field at 2 K. (d) FFT spectrum of the bulk CsV_3Sb_5 for the data between 4 T to 14 T. The inset shows the oscillatory signals after the removal of the background. (e) FFT spectrum of the same bulk sample for the data between 8.5 T to 14 T. The inset shows the oscillatory signals after the removal of the background.

transition. With a further cooling, $\rho(T)$ shows the onset of the superconducting transition at ~ 3.7 K (see the lower inset in Fig. 1(a)). The RRR of this sample is ~ 118 , currently one of the highest reported values. With the availability of high-quality single crystals, we further measure the magnetoresistance at the base temperature (2 K) with $B \parallel c$ up to 14 T. As displayed in Fig. 1(c), pronounced SdH oscillations can be discerned from the raw data even without removing the background. The fast Fourier transformation (FFT) spectrum in Fig. 1(d) shows four peaks (12 T, 24 T, 73 T and 88 T) below 100 T with an excellent signal-to-noise ratio, which agree well with other groups’ results^{28,41,42}. In addition, we also detect some weak oscillatory signals between 500 T and 2000 T, as displayed in Fig. 1(e). Notably, we successfully

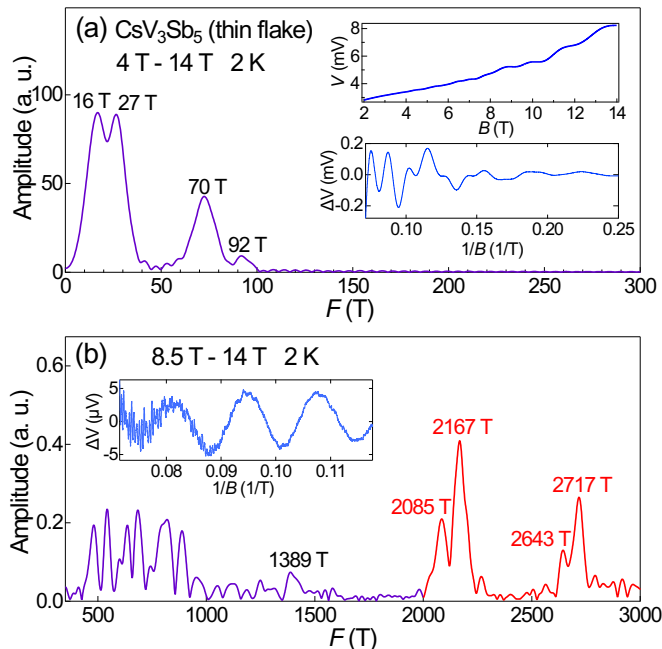


FIG. 2. (a) FFT spectrum of the thin flake (800 nm) for the data between 4 T to 14 T collected at 2 K. The upper inset is the raw data of the voltage against magnetic field. The lower inset shows the oscillatory signals after removing the background. (b) FFT spectrum of the same flake for the data between 8.5 T to 14 T. The two new groups of peaks discovered in this work are highlighted in red. The inset shows the oscillatory signals after removing the background.

capture one QO frequency of 2079 T, which is close to the largest frequency reported in Ref. 46. Similar to previous studies, the peak amplitudes in the mid-frequency spectrum are significantly less intense than those in the low-frequency spectrum.

B. Discovery of high-frequency peaks in thin flakes

The highly conductive nature of our sample unavoidably makes the resistive signal extremely weak at low temperatures. To enhance the signal-to-noise ratio, we study a thin flake cleaved from the same bulk sample, thereby providing a more favourable geometric factor. Using a technique recently developed by some of us⁴⁷, we successfully transfer a flake of CsV₃Sb₅ with a thickness of 800 nm onto a diamond substrate pre-patterned with electrodes. The diamond substrate provides an ideal platform to ensure that the flake is thermally anchored to the cold head. As presented in Supplemental Material⁴⁸, both the CDW and sharp superconducting transitions can be observed in the thin flake, but T_{CDW} decreases to around 84 K and T_c increases to ~ 4.6 K. This is probably because the flake experiences a strain from the substrate, or more intriguingly, the thin flake's carrier concentration has been modified due to air exposure⁵².

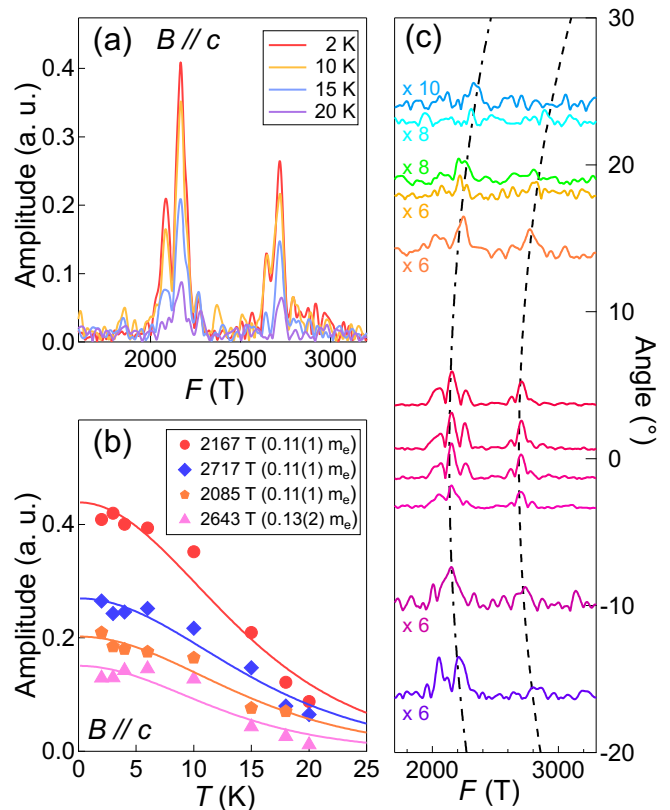


FIG. 3. (a) FFT spectra of SdH oscillations at different temperatures. (b) Temperature dependence of the SdH amplitudes for the peaks at 2085 T, 2167 T, 2643 T and 2717 T (solid symbols). The solid curves are fits using the thermal damping factor R_T . (c) FFT spectra of SdH oscillations at several field angles (θ). The simulations via $F(\theta) = F(0^\circ)/\cos\theta$ are shown, with $F(0^\circ) = 2135$ T and 2687 T for the dash-dotted and the dashed curves, respectively. $\theta = 0^\circ$ corresponds to the c -axis, and the rotation is towards the ab -plane. FFT spectra at high angles have their amplitudes amplified by factors ranging from 6 to 10.

We conduct the magnetoresistance measurement for the thin flake of CsV₃Sb₅ and the upper inset of Fig. 2(a) shows the voltage recorded by the lock-in amplifier against the magnetic field at 2 K. The magnetic field is parallel to the c -axis. Figure 2(a) displays the FFT spectrum for the data between 4 T and 14 T and four peaks (at 16 T, 27 T, 70 T and 92 T) are resolved, which are consistent with the observation in our bulk crystal and the reported values in bulk crystals by other groups^{28,41,42}. This, once again, highlights the satisfactory consistency for the low-frequency spectrum. Besides, we detect a group of peaks between 400 T and 1000 T and one peak of 1389 T with good signal-to-noise ratio, as shown in Fig. 2(b). This mid-frequency group has also been reported earlier^{42,46}. These frequencies readily have some correspondence in our DFT calculations, although their definite assignment is beyond the scope of the present work.

Surprisingly, we find two new groups of peaks with rather high frequencies (2085 T and 2167 T, 2643 T and 2717 T, highlighted in red in Fig. 2(b)) with an excellent signal-to-noise ratio. To the best of our knowledge, this is the first observation of QO with frequencies far beyond 2000 T in CsV₃Sb₅ when $B \parallel c$, offering a precious opportunity to expand our fermiology knowledge of CsV₃Sb₅. The high-frequency spectrum shows sensitivity to both the temperature and the field angle (Fig. 3). With an increasing temperature, the dominant peaks become less intense. From the thermal damping term of the Lifshitz-Kosevich theory, $R_T = X/\sinh X$ with $X = 14.693m^*T/B$, the cyclotron effective mass can be extracted from the temperature dependence of the QO amplitude. As analyzed in Fig. 3(b), m^* for the peaks at 2085 T, 2167 T, 2643 T and 2717 T are found to be 0.11(1) m_e , 0.11(1) m_e , 0.13(2) m_e and 0.11(1) m_e , respectively. The relatively small m^* for these four high-frequency peaks reflect the quasi-linear nature of the relevant electronic bands. Furthermore, the Fermi velocity (v_F) calculated from $m^*v_F = \hbar k_F$ is rather large. Approximating the orbits as circles with radii k_F , v_F ranges from 2.53×10^6 m/s to 3.03×10^6 m/s for these high-frequency peaks. These values are roughly one order-of-magnitude higher than typical topological insulators^{53–56}.

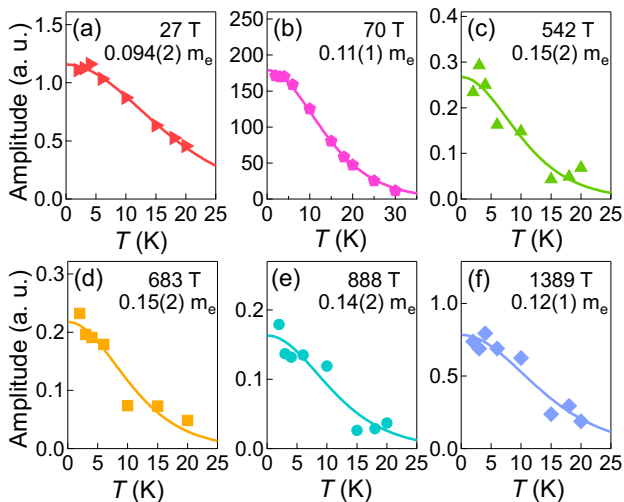


FIG. 4. Temperature dependence of QO amplitudes for the frequencies of 27 T, 70 T, 542 T, 683 T, 888 T and 1389 T in the thin flake of CsV₃Sb₅. The solid curves are the fit using the thermal damping factor of Lifshitz-Kosevich theory. The effective masses extracted are 0.094(2) m_e (27 T), 0.11(1) m_e (70 T), 0.15(2) m_e (542 T), 0.15(2) m_e (683 T), 0.14(2) m_e (888 T), 0.12(1) m_e (1389 T).

Figure 3(c) shows the FFT spectra at selected magnetic field angles, focusing on the high-frequency region. When the angle between the sample c -axis and the magnetic field direction (θ) is large, the signal becomes weaker and therefore multiple field sweeps under identi-

cal conditions are collected to accumulate enough signals, a methodology that we successfully employed to resolve weak QO frequencies in MoTe₂ under pressure⁴⁰. For instance, the FFT spectrum at 23.6° is the result of averaging 4 sweeps. As θ increases, the QO frequencies increase according to $F(\theta) = F(0^\circ)/\cos \theta$ (see the simulations for the stronger peaks illustrated in Fig. 3(c)). Such an angular dependence is a typical behaviour of quasi-2D Fermi surfaces, suggesting that the high-frequency peaks come from quasi-2D Fermi surfaces⁵⁷.

C. Effective masses of other peaks in thin flakes

In addition to the high-frequency group, our relatively high signal-to-noise ratio enables the determination of the cyclotron effective mass (m^*) for other peaks. Figure 4 shows the temperature dependence of the QO amplitudes (solid symbols) for six other relatively more intense peaks. The analysis using the thermal damping factor R_T (solid curves) gives the m^* of 0.094(2) m_e , 0.11(1) m_e , 0.15(2) m_e , 0.15(2) m_e , 0.14(2) m_e and 0.12(1) m_e for 27 T, 70 T, 542 T, 683 T, 888 T and 1389 T respectively.

The m^* values for the 27 T and 70 T peaks are consistent with the reported values in bulk crystals^{41,42}. For 542 T, 683 T, 888 T and 1389 T, m^* values are generally smaller than the reported values associated with comparable frequencies in Ref. 46.

D. High-frequency peaks in other flakes

To prove the existence of high-frequency quantum oscillations in thin flakes, we prepare two other flakes following the same experimental procedures. The first flake (#B) was cleaved from another piece of crystal from the same batch as the ones presented in Fig. 2, while the second flake (#C) was extracted from a crystal from an entirely different batch. The thicknesses of #B and of #C are 700 nm and 500 nm, respectively.

As shown in Figs. 5(a) and 5(b), the FFT spectra of the new flakes are consistent with Fig. 2(b) and we successfully resolve the two groups of high frequencies. The robustness of these high-frequency oscillations and our ability to reproduce them in completely different thin flakes suggest that they are the intrinsic feature.

IV. DISCUSSION

To understand the fermiology of CsV₃Sb₅, we perform band structure calculations. The precise nature of the CDW state is currently under debate, but it is generally accepted that the CDW state is accompanied by an in-plane distortion which results in a 2×2 in-plane superstructure. Candidate distortion modes consistent with such a superstructure include a ‘Star of David’

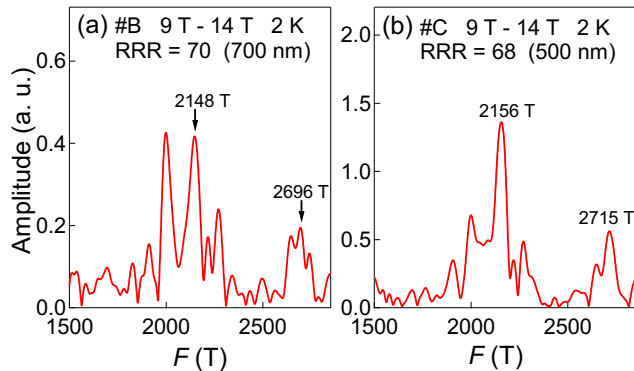


FIG. 5. FFT spectra of SdH quantum oscillations for (a) flake #B (700 nm) and (b) flake #C (500 nm).

(SoD) and a tri-hexagonal (TrH) deformation of vanadium layers^{42,58}. X-ray diffraction, second harmonic generation measurements and Raman spectroscopy^{20,42} further revealed additional out-of-plane structural modulations, in which both TrH and SoD layers stack to increase the periodicity to 4 layers. This is commonly referred to as $2 \times 2 \times 4$ distortion.

To correctly analyze the QO spectra, band foldings must be taken into account as the increased real space periodicity introduced by the CDW order reconstructs the Fermi surfaces. We have calculated the band structure of CsV_3Sb_5 for the $2 \times 2 \times 4$ distortion. The in-plane Brillouin zone has an area equivalent to a QO frequency of ~ 4040 T, large enough to contain the orbits associated with the detected high-frequency peaks when $B \parallel c$. The calculated band structure is complicated, resulting in 17 Fermi surface sheets. The largest calculated frequency is associated with the quasi-2D Fermi surface sheet displayed in Fig. 6(a), while the remaining sheets are presented in Supplemental Material⁴⁸. The corresponding extremal orbit is depicted in Fig. 6(b). The ‘as-calculated’ value of 1690 T for the largest frequency is still somewhat smaller than the experimental observations.

Magnetic breakdown has been shown to be active in CsV_3Sb_5 ⁴⁴, and it is natural to ask if the high-frequency peaks discovered here can be attributed to magnetic breakdown. The complicated Fermi surfaces with multiple sheets in close proximity also make the system prone to magnetic breakdown. When quantum oscillation frequencies combine, the effective mass of the resultant frequency is the sum of the effective masses of the constituent components. Consider the simplest case involving only two frequencies, the effective mass of the ‘breakdown orbit’ described by $(F_1 + F_2)$ satisfies $m^*(F_1 + F_2) = m^*(F_1) + m^*(F_2)$ ^{59,60}.

Given that m^* of the high-frequency peaks are very similar to m^* of the peaks with lower frequencies, magnetic breakdown cannot be applied here. For example, 2085 T is close to the sum of 683 T and 1389 T. How-

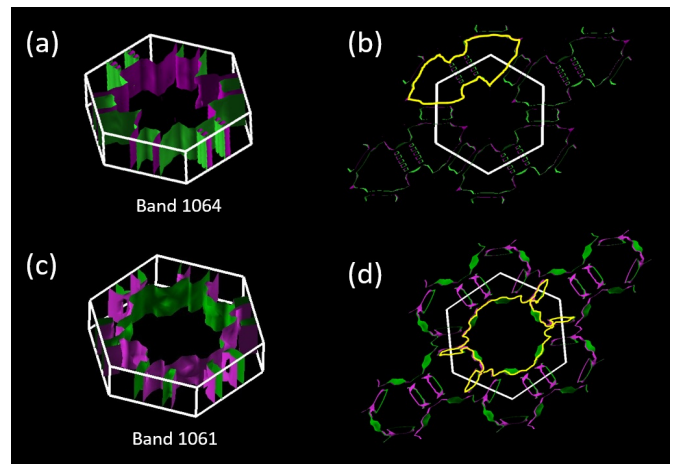


FIG. 6. (a,b) The Fermi surface sheet that hosts the largest extremal orbit when $B \parallel c$. The orbit is shown in yellow, which gives a QO frequency of 1690 T. The white border shows the Brillouin zone boundary. (c,d) After shifting E_F downward, another Fermi surface sheet hosts the largest extremal orbit when $B \parallel c$. The orbit corresponds to a QO frequency of 1940 T. The illustrations in (b) and (d) are viewed along the k_z -axis.

ever, $m^*(683 \text{ T}) + m^*(1389 \text{ T}) = 0.27(3) m_e$, significantly larger than $m^*(2085 \text{ T}) = 0.11(1) m_e$. With the identical argument, we can also rule out the possibility that the high-frequency oscillations are harmonics.

We point out that the true value of the Fermi energy (E_F) can be different from the obtained value in the calculations, and it has been pointed out that the QO frequencies are very sensitive to E_F ⁴². Hence, to reconcile the mismatch between the experimental and the calculated frequencies, we investigate the mechanism that can affect E_F of our sample.

The usage of a thin flake to boost the signal-to-noise ratio offers a clue. In the scenario of ‘orbital-selective hole doping’ proposed recently^{52,61}, the surface of CsV_3Sb_5 can be slightly oxidized when exposed to air. The net result is the hole doping of certain orbitals, leading to a relative downward shift of E_F with respect to the bands formed by the overlap of these orbitals. Therefore, orbital-selective mechanism can lead to the increase of some QO frequencies. The effect is more pronounced in thinner samples because of the increasing surface-to-volume ratio upon thinning. It is imperative to note that not all orbitals are affected by the shift (hence the term ‘orbital-selective’), potentially explaining the better agreement between the flake and the bulk crystals in the low-frequency and the mid-frequency parts of the QO spectra. Song *et al.* shows that a Cs deficiency of 5% can give a relative band shift on the order of 100 meV for some bands⁵². As an illustration, we manually shift E_F downward by 58 meV, keeping the entire band structure intact. Such an operation results in a maximum frequency of 1940 T (Fig. 6(d)), hosted by another Fermi

surface sheet shown in Fig. 6(c). To quantitatively explain our data, the precise hole concentration and a more realistic calculation that only shifts certain bands are needed. Nevertheless, our data clearly support the picture of the orbital selective hole doping in the thin flake. The hole doping readily supports the observed higher T_c in our thin flake, which is also consistent with the previous report⁵². Therefore, orbital-selective carrier doping is an attractive avenue to modify the carrier concentration as well as the superconducting properties of CsV_3Sb_5 .

V. CONCLUSION

To summarize, we have investigated the fermiology of CsV_3Sb_5 using Shubnikov-de Haas quantum oscillations. In our thin flake, we detect new frequencies associated with large extremal orbits ranging from ~ 2085 T to ~ 2717 T, all with surprisingly low effective masses of $\sim 0.1 m_e$. The large number of high-velocity carriers revealed by our study will give new insights for understanding the exotic quantum transport properties in CsV_3Sb_5 . Combining with the DFT calculations, we consider the $2 \times 2 \times 4$ distortion for determining the folded Fermi surface in the CDW phase. We argue that an orbital-

selective modification of charge carriers can be a promising mechanism to explain the new groups of high frequency quantum oscillations. Our work not only demonstrates the rich feature of the fermiology of CsV_3Sb_5 , but also supports the idea of the orbital-selective mechanism as an effective way to tune the electronic properties of kagome superconductors AV_3Sb_5 .

Note added. When we were finalizing our manuscript, we became aware of a preprint which reports pulsed-field quantum oscillation data up to 86 T in CsV_3Sb_5 ⁶². Quantum oscillation frequencies beyond 2 kT have been observed, and some of these frequencies have been attributed to magnetic breakdown⁶². This interpretation is dissimilar to ours.

ACKNOWLEDGMENTS

We acknowledge Wai Kin Wong for experimental support. The work was supported by Research Grants Council of Hong Kong (CUHK 14300418, CUHK 14300117, CUHK 14300419, CUHK 14301020, A-CUHK 402/19), CUHK Direct Grant (4053408, 4053461, 4053463), the National Natural Science Foundation of China (12104384), and CityU Start-up Grant (No. 9610438).

[§]W.Z. and L.W. contributed equally to this work.

* wingcyu@cityu.edu.hk

† ktlai@phy.cuhk.edu.hk

‡ skgoh@cuhk.edu.hk

¹ Y. Zhou, K. Kanoda, and T.-K. Ng, “Quantum spin liquid states,” *Rev. Mod. Phys.* **89**, 025003 (2017).

² M. L. Kiesel and R. Thomale, “Sublattice interference in the kagome Hubbard model,” *Phys. Rev. B* **86**, 121105 (2012).

³ M. L. Kiesel, C. Platt, and R. Thomale, “Unconventional Fermi surface instabilities in the kagome Hubbard model,” *Phys. Rev. Lett.* **110**, 126405 (2013).

⁴ W.-S. Wang, Z.-Z. Li, Y.-Y. Xiang, and Q.-H. Wang, “Competing electronic orders on kagome lattices at van Hove filling,” *Phys. Rev. B* **87**, 115135 (2013).

⁵ Q. Wang, Y. Xu, R. Lou, Z. Liu, M. Li, Y. Huang, D. Shen, H. Weng, S. Wang, and H. Lei, “Large intrinsic anomalous Hall effect in half-metallic ferromagnet $\text{Co}_3\text{Sn}_2\text{S}_2$ with magnetic Weyl fermions,” *Nat Commun.* **9**, 3681 (2018).

⁶ B. R. Ortiz, L. C. Gomes, J. R. Morey, M. Winiarski, M. Bordelon, J. S. Mangum, I. W. H. Oswald, J. A. Rodriguez-Rivera, J. R. Neilson, S. D. Wilson, E. Ertekin, T. M. McQueen, and E. S. Toberer, “New kagome prototype materials: discovery of KV_3Sb_5 , RbV_3Sb_5 , and CsV_3Sb_5 ,” *Phys. Rev. Mater.* **3**, 094407 (2019).

⁷ T. Neupert, M. M. Denner, J.-X. Yin, R. Thomale, and M. Z. Hasan, “Charge order and superconductivity in kagome materials,” *Nat. Phys.* **18**, 137 (2021).

⁸ F. Du, S. Luo, B. R. Ortiz, Y. Chen, W. Duan, D. Zhang, X. Lu, S. D. Wilson, Y. Song, and H. Yuan, “Pressure-induced double superconducting domes and charge instability in the kagome metal KV_3Sb_5 ,” *Phys. Rev. B* **103**,

L220504 (2021).

⁹ K. Y. Chen, N. N. Wang, Q. W. Yin, Y. H. Gu, K. Jiang, Z. J. Tu, C. S. Gong, Y. Uwatoko, J. P. Sun, H. C. Lei, J. P. Hu, and J.-G. Cheng, “Double superconducting dome and triple enhancement of T_c in the kagome superconductor CsV_3Sb_5 under high pressure,” *Phys. Rev. Lett.* **126**, 247001 (2021).

¹⁰ H. Li, T. T. Zhang, T. Yilmaz, Y. Y. Pai, C. E. Marvinney, A. Said, Q. W. Yin, C. S. Gong, Z. J. Tu, E. Vescovo, C. S. Nelson, R. G. Moore, S. Murakami, H. C. Lei, H. N. Lee, B. J. Lawrie, and H. Miao, “Observation of unconventional charge density wave without acoustic phonon anomaly in kagome superconductors AV_3Sb_5 ($A = \text{Rb}, \text{Cs}$),” *Phys. Rev. X* **11**, 031050 (2021).

¹¹ Z. Liang, X. Hou, F. Zhang, W. Ma, P. Wu, Z. Zhang, F. Yu, J.-J. Ying, K. Jiang, L. Shan, Z. Wang, and X.-H. Chen, “Three-dimensional charge density wave and surface-dependent vortex-core states in a kagome superconductor CsV_3Sb_5 ,” *Phys. Rev. X* **11**, 031026 (2021).

¹² H. Zhao, H. Li, B. R. Ortiz, S. M. L. Teicher, T. Park, M. Ye, Z. Wang, L. Balents, S. D. Wilson, and I. Zeljkovic, “Cascade of correlated electron states in the kagome superconductor CsV_3Sb_5 ,” *Nature* **599**, 216 (2021).

¹³ Z. Liu, N. Zhao, Q. Yin, C. Gong, Z. Tu, M. Li, W. Song, Z. Liu, D. Shen, Y. Huang, K. Liu, H. Lei, and S. Wang, “Charge-density-wave-induced bands renormalization and energy gaps in a kagome superconductor RbV_3Sb_5 ,” *Phys. Rev. X* **11**, 041010 (2021).

¹⁴ Y. Hu, S. M. L. Teicher, B. R. Ortiz, Y. Luo, S. Peng, L. Huai, J. Z. Ma, N. C. Plumb, S. D. Wilson, J. F. He, and M. Shi, “Charge-order-assisted topological surface states

- and flat bands in the kagome superconductor CsV_3Sb_5 ,” arXiv:2104.12725 (2021).
- 15 E. Uykur, B. R. Ortiz, S. D. Wilson, M. Dressel, and A. A. Tsirlin, “Optical detection of the density-wave instability in the kagome metal KV_3Sb_5 ,” npj Quantum Mater. **7**, 16 (2022).
 - 16 X. Zhou, Y. Li, X. Fan, J. Hao, Y. Dai, Z. Wang, Y. Yao, and H.-H. Wen, “Origin of charge density wave in the kagome metal CsV_3Sb_5 as revealed by optical spectroscopy,” Phys. Rev. B **104**, L041101 (2021).
 - 17 Y.-X. Jiang, J.-X. Yin, M. M. Denner, N. Shumiya, B. R. Ortiz, G. Xu, Z. Guguchia, J. He, M. S. Hossain, X. Liu, J. Ruff, L. Kautzsch, S. S. Zhang, G. Chang, I. Belopolski, Q. Zhang, T. A. Cochran, D. Multer, M. Litskevich, Z.-J. Cheng, X. P. Yang, Z. Wang, R. Thomale, T. Neupert, S. D. Wilson, and M. Z. Hasan, “Unconventional chiral charge order in kagome superconductor KV_3Sb_5 ,” Nat. Mater. **20**, 1353 (2021).
 - 18 M. Kang, S. Fang, J.-K. Kim, B. R. Ortiz, S. H. Ryu, J. Kim, J. Yoo, G. Sangiovanni, D. Di Sante, B.-G. Park, C. Jozwiak, A. Bostwick, E. Rotenberg, E. Kaxiras, S. D. Wilson, J.-H. Park, and R. Comin, “Twofold van Hove singularity and origin of charge order in topological kagome superconductor CsV_3Sb_5 ,” Nat. Phys. **18**, 301 (2022).
 - 19 M. Kang, S. Fang, J. Yoo, B. R. Ortiz, Y. Oey, S. H. Ryu, J. Kim, C. Jozwiak, A. Bostwick, E. Rotenberg, E. Kaxiras, J. Checkelsky, S. D. Wilson, J.-H. Park, and R. Comin, “Microscopic structure of three-dimensional charge order in kagome superconductor AV_3Sb_5 and its tunability,” arXiv:2202.01902 (2022).
 - 20 S. Wu, B. R. Ortiz, H. Tan, S. D. Wilson, B. Yan, T. Birol, and G. Blumberg, “Charge density wave order in kagome metal AV_3Sb_5 (A = Cs, Rb, K),” arXiv:2201.05188 (2022).
 - 21 R. Lou, A. Fedorov, Q. Yin, A. Kuibarov, Z. Tu, C. Gong, E. F. Schwier, B. Büchner, H. Lei, and S. Borisenko, “Charge-density-wave-induced peak-dip-hump structure and the multiband superconductivity in a kagome superconductor CsV_3Sb_5 ,” Phys. Rev. Lett. **128**, 036402 (2022).
 - 22 Z. Wang, Y.-X. Jiang, J.-X. Yin, Y. Li, G.-Y. Wang, H.-L. Huang, S. Shao, J. Liu, P. Zhu, N. Shumiya, M. S. Hossain, H. Liu, Y. Shi, J. Duan, X. Li, G. Chang, P. Dai, Z. Ye, G. Xu, Y. Wang, H. Zheng, J. Jia, M. Z. Hasan, and Y. Yao, “Electronic nature of chiral charge order in the kagome superconductor CsV_3Sb_5 ,” Phys. Rev. B **104**, 075148 (2021).
 - 23 N. Shumiya, M. S. Hossain, J.-X. Yin, Y.-X. Jiang, B. R. Ortiz, H. Liu, Y. Shi, Q. Yin, H. Lei, S. S. Zhang, G. Chang, Q. Zhang, T. A. Cochran, D. Multer, M. Litskevich, Z.-J. Cheng, X. P. Yang, Z. Guguchia, S. D. Wilson, and M. Z. Hasan, “Intrinsic nature of chiral charge order in the kagome superconductor RbV_3Sb_5 ,” Phys. Rev. B **104**, 035131 (2021).
 - 24 C. Mielke III, D. Das, J. X. Yin, H. Liu, R. Gupta, Y. X. Jiang, M. Medarde, X. Wu, H. C. Lei, J. Chang, P. Dai, Q. Si, H. Miao, R. Thomale, T. Neupert, Y. Shi, R. Khasanov, M. Z. Hasan, H. Luetkens, and Z. Guguchia, “Time-reversal symmetry-breaking charge order in a kagome superconductor,” Nature **602**, 245 (2022).
 - 25 L. Yu, C. Wang, Y. Zhang, M. Sander, S. Ni, Z. Lu, S. Ma, Z. Wang, Z. Zhao, H. Chen, K. Jiang, Y. Zhang, H. Yang, F. Zhou, X. Dong, S. L. Johnson, M. J. Graf, J. Hu, H.-J. Gao, and Z. Zhao, “Evidence of a hidden flux phase in the topological kagome metal CsV_3Sb_5 ,” arXiv:2107.10714 (2021).
 - 26 X. Feng, K. Jiang, Z. Wang, and J. Hu, “Chiral flux phase in the kagome superconductor AV_3Sb_5 ,” Sci. Bull. **66**, 1384 (2021).
 - 27 S.-Y. Yang, Y. Wang, B. R. Ortiz, D. Liu, J. Gayles, E. Derunova, R. Gonzalez-Hernandez, L. Šmejkal, Y. Chen, S. S. P. Parkin, S. D. Wilson, E. S. Toberer, T. McQueen, and M. N. Ali, “Giant, unconventional anomalous Hall effect in the metallic frustrated magnet candidate, KV_3Sb_5 ,” Sci. Adv. **6**, eabb6003 (2020).
 - 28 F. H. Yu, T. Wu, Z. Y. Wang, B. Lei, W. Z. Zhuo, J. J. Ying, and X. H. Chen, “Concurrence of anomalous Hall effect and charge density wave in a superconducting topological kagome metal,” Phys. Rev. B **104**, L041103 (2021).
 - 29 G. Zheng, Z. Chen, C. Tan, M. Wang, X. Zhu, S. Albarakati, M. Algarni, J. Partridge, L. Farrar, J. Zhou, W. Ning, M. Tian, M. S. Fuhrer, and L. Wang, “Gate-controllable giant anomalous Hall effect from flat bands in kagome metal CsV_3Sb_5 nanoflakes,” arXiv:2109.12588 (2021).
 - 30 B. R. Ortiz, S. M. L. Teicher, Y. Hu, J. L. Zuo, P. M. Sarte, E. C. Schueller, A. M. M. Abeykoon, M. J. Krogstad, S. Rosenkranz, R. Osborn, R. Seshadri, L. Balents, J. He, and S. D. Wilson, “ CsV_3Sb_5 : A \mathbb{Z}_2 topological kagome metal with a superconducting ground state,” Phys. Rev. Lett. **125**, 247002 (2020).
 - 31 B. R. Ortiz, P. M. Sarte, E. M. Kenney, M. J. Graf, S. M. L. Teicher, R. Seshadri, and S. D. Wilson, “Superconductivity in the \mathbb{Z}_2 kagome metal KV_3Sb_5 ,” Phys. Rev. Mater. **5**, 034801 (2021).
 - 32 Q. Yin, Z. Tu, C. Gong, Y. Fu, S. Yan, and H. Lei, “Superconductivity and normal-state properties of kagome metal RbV_3Sb_5 single crystals,” Chin. Phys. Lett. **38**, 037403 (2021).
 - 33 F. Yu, D. Ma, W. Zhuo, S. Liu, X. Wen, B. Lei, J. Ying, and X. Chen, “Unusual competition of superconductivity and charge-density-wave state in a compressed topological kagome metal,” Nat. Commun. **12**, 3645 (2021).
 - 34 Q. Wang, P. Kong, W. Shi, C. Pei, C. Wen, L. Gao, Y. Zhao, Q. Yin, Y. Wu, G. Li, H. Lei, J. Li, Y. Chen, S. Yan, and Y. Qi, “Charge density wave orders and enhanced superconductivity under pressure in the kagome metal CsV_3Sb_5 ,” Adv. Mater. **33**, 2102813 (2021).
 - 35 Z. Zhang, Z. Chen, Y. Zhou, Y. Yuan, S. Wang, J. Wang, H. Yang, C. An, L. Zhang, X. Zhu, Y. Zhou, X. Chen, J. Zhou, and Z. Yang, “Pressure-induced reemergence of superconductivity in the topological kagome metal CsV_3Sb_5 ,” Phys. Rev. B **103**, 224513 (2021).
 - 36 N. N. Wang, K. Y. Chen, Q. W. Yin, Y. N. N. Ma, B. Y. Pan, X. Yang, X. Y. Ji, S. L. Wu, P. F. Shan, S. X. Xu, Z. J. Tu, C. S. Gong, G. T. Liu, G. Li, Y. Uwatoko, X. L. Dong, H. C. Lei, J. P. Sun, and J.-G. Cheng, “Competition between charge-density-wave and superconductivity in the kagome metal RbV_3Sb_5 ,” Phys. Rev. Res. **3**, 043018 (2021).
 - 37 F. Han, J. Xu, A. S. Botana, Z. L. Xiao, Y. L. Wang, W. G. Yang, D. Y. Chung, M. G. Kanatzidis, M. R. Norman, G. W. Crabtree, and W. K. Kwok, “Separation of electron and hole dynamics in the semimetal LaSb ,” Phys. Rev. B **96**, 125112 (2017).
 - 38 Y. J. Hu, E. I. P. Aulestia, K. F. Tse, C. N. Kuo, J. Y. Zhu, C. S. Lue, K. T. Lai, and S. K. Goh, “Extremely large magnetoresistance and the complete determination of the Fermi surface topology in the semimetal ScSb ,” Phys. Rev.

- B **98**, 035133 (2018).
- ³⁹ D. Rhodes, R. Schönemann, N. Aryal, Q. Zhou, Q. R. Zhang, E. Kampert, Y.-C. Chiu, Y. Lai, Y. Shimura, G. T. McCandless, J. Y. Chan, D. W. Paley, J. Lee, A. D. Finke, J. P. C. Ruff, S. Das, E. Manousakis, and L. Balicas, “Bulk Fermi surface of the Weyl type-II semimetallic candidate γ -MoTe₂,” *Phys. Rev. B* **96**, 165134 (2017).
- ⁴⁰ Y. J. Hu, W. C. Yu, K. T. Lai, D. Sun, F. F. Balakirev, W. Zhang, J. Y. Xie, K. Y. Yip, E. I. P. Aulestia, R. Jha, R. Higashinaka, T. D. Matsuda, Y. Yanase, Y. Aoki, and S. K. Goh, “Detection of hole pockets in the candidate type-II Weyl semimetal MoTe₂ from Shubnikov–de Haas quantum oscillations,” *Phys. Rev. Lett.* **124**, 076402 (2020).
- ⁴¹ Y. Fu, N. Zhao, Z. Chen, Q. Yin, Z. Tu, C. Gong, C. Xi, X. Zhu, Y. Sun, K. Liu, and H. Lei, “Quantum transport evidence of topological band structures of kagome superconductor CsV₃Sb₅,” *Phys. Rev. Lett.* **127**, 207002 (2021).
- ⁴² B. R. Ortiz, S. M. Teicher, L. Kautzsch, P. M. Sarte, N. Ratcliff, J. Harter, J. P. Ruff, R. Seshadri, and S. D. Wilson, “Fermi surface mapping and the nature of charge-density-wave order in the kagome superconductor CsV₃Sb₅,” *Phys. Rev. X* **11**, 041030 (2021).
- ⁴³ Y. Gan, W. Xia, L. Zhang, K. Yang, X. Mi, A. Wang, Y. Chai, Y. Guo, X. Zhou, and M. He, “Magneto-Seebeck effect and ambipolar Nernst effect in the CsV₃Sb₅ superconductor,” *Phys. Rev. B* **104**, L180508 (2021).
- ⁴⁴ D. Chen, B. He, M. Yao, Y. Pan, H. Lin, W. Schnelle, Y. Sun, J. Gooth, L. Taillefer, and C. Felser, “Anomalous thermoelectric effects and quantum oscillations in the kagome metal CsV₃Sb₅,” *Phys. Rev. B* **105**, L201109 (2022).
- ⁴⁵ X. Huang, C. Guo, C. Putzke, M. Gutierrez-Amigo, Y. Sun, M. G. Vergniory, I. Errea, D. Chen, C. Felser, and P. J. W. Moll, “Three-dimensional Fermi surfaces from charge order in layered CsV₃Sb₅,” *Phys. Rev. B* **106**, 064510 (2022).
- ⁴⁶ K. Shrestha, R. Chapai, B. K. Pokharel, D. Miertschin, T. Nguyen, X. Zhou, D. Y. Chung, M. G. Kanatzidis, J. F. Mitchell, U. Welp, D. Popović, D. E. Graf, B. Lorenz, and W. K. Kwok, “Nontrivial Fermi surface topology of the kagome superconductor CsV₃Sb₅ probed by de Haas–van Alphen oscillations,” *Phys. Rev. B* **105**, 024508 (2022).
- ⁴⁷ J. Xie, X. Liu, W. Zhang, S. M. Wong, X. Zhou, Y. Zhao, S. Wang, K. T. Lai, and S. K. Goh, “Fragile pressure-induced magnetism in FeSe superconductors with a thickness reduction,” *Nano Lett.* **21**, 9310 (2021).
- ⁴⁸ See Supplemental Material for (i) details of density functional theory calculations, (ii) temperature dependence of electrical resistivity for a thin flake of CsV₃Sb₅, (iii) calculated Fermi surfaces for the distorted CsV₃Sb₅ ($2 \times 2 \times 4$ superstructure). The Supplemental Material includes additional Refs. [49–51].
- ⁴⁹ K. Schwarz and P. Blaha, “Solid state calculations using WIEN2k,” *Comput. Mater. Sci.* **28**, 259 (2003).
- ⁵⁰ J. P. Perdew, K. Burke, and M. Ernzerhof, “Generalized gradient approximation made simple,” *Phys. Rev. Lett.* **77**, 3865 (1996).
- ⁵¹ P. Rourke and S. Julian, “Numerical extraction of de Haas–van Alphen frequencies from calculated band energies,” *Comput. Phys. Commun.* **183**, 324 (2012).
- ⁵² Y. Song, T. Ying, X. Chen, X. Han, X. Wu, A. P. Schnyder, Y. Huang, J.-G. Guo, and X. Chen, “Competition of superconductivity and charge density wave in selective oxidized CsV₃Sb₅ thin flakes,” *Phys. Rev. Lett.* **127**, 237001 (2021).
- ⁵³ D.-X. Qu, Y. S. Hor, J. Xiong, R. J. Cava, and N. P. Ong, “Quantum oscillations and Hall anomaly of surface states in the topological insulator Bi₂Te₃,” *Science* **329**, 821 (2010).
- ⁵⁴ A. Taskin, Z. Ren, S. Sasaki, K. Segawa, and Y. Ando, “Observation of Dirac holes and electrons in a topological insulator,” *Phys. Rev. Lett.* **107**, 016801 (2011).
- ⁵⁵ J. G. Analytis, R. D. McDonald, S. C. Riggs, J.-H. Chu, G. Boebinger, and I. R. Fisher, “Two-dimensional surface state in the quantum limit of a topological insulator,” *Nat. Phys.* **6**, 960 (2010).
- ⁵⁶ H.-S. Kim, T.-H. Hwang, N.-H. Kim, Y. Hou, D. Yu, H.-S. Sim, and Y.-J. Doh, “Adjustable quantum interference oscillations in Sb-doped Bi₂Se₃ topological insulator nanoribbons,” *ACS nano* **14**, 14118 (2020).
- ⁵⁷ We take the 2167 T frequency as an example. For the ease of argument, we assume a circular orbit in the k_x - k_y plane. The 2167 T frequency follows $F(\theta) = F(0^\circ)/\cos\theta$ well up to 23.6° and at 23.6° , the ‘ k_z -height’ of the extremal orbit associated with the 2167 T frequency is around 0.224 \AA^{-1} , which is much larger than the height of the first Brillouin zone (0.168 \AA^{-1} for the $2 \times 2 \times 4$ superstructure). At 23.6° , the quantum oscillation orbit has already traveled beyond the first Brillouin zone and the Fermi surface is never closed. Hence, even with data up to 23.6° only, we can safely conclude the quasi-2D nature of this Fermi surface sheet.
- ⁵⁸ H. Tan, Y. Liu, Z. Wang, and B. Yan, “Charge density waves and electronic properties of superconducting kagome metals,” *Phys. Rev. Lett.* **127**, 046401 (2021).
- ⁵⁹ D. Shoenberg, *Magnetic Oscillations in Metals*. (Cambridge Univ. Press, 1984).
- ⁶⁰ S. Friedemann, S. K. Goh, P. M. C. Rourke, P. Reiss, M. L. Sutherland, F. M. Grosche, G. Zwicknagl, and Z. Fisk, “Electronic structure of LuRh₂Si₂: ‘small’ fermi surface reference to YbRh₂Si₂,” *New J. Phys.* **15**, 093014 (2013).
- ⁶¹ Y. Luo, S. Peng, S. M. L. Teicher, L. Huai, Y. Hu, B. R. Ortiz, Z. Wei, J. Shen, Z. Ou, B. Wang, Y. Miao, M. Guo, M. Shi, S. D. Wilson, and J. F. He, “Distinct band reconstructions in kagome superconductor CsV₃Sb₅,” arXiv:2106.01248 (2021).
- ⁶² R. Chapai, M. Leroux, V. Oliviero, D. Vignolles, M. Smylie, D. Chung, M. Kanatzidis, W.-K. Kwok, J. Mitchell, and U. Welp, “Magnetic breakdown and topology in the kagome superconductor CsV₃Sb₅ under high magnetic field,” arXiv:2208.05523 (2022).